Draft version February 7, 2022
Typeset using LaTeX **twocolumn** style in AASTeX63

arXiv:2009.03342v1 [physics.plasm-ph] 7 Sep 2020

As a matter of tension – kinetic energy spectra in MHD turbulence

Philipp Grete,[1] Brian W. O'Shea,[1,2,3] and Kris Beckwith[4]

[1] *Department of Physics and Astronomy, Michigan State University, East Lansing, MI 48824, USA*
[2] *Department of Computational Mathematics, Science and Engineering, Michigan State University, East Lansing, MI 48824, USA*
[3] *National Superconducting Cyclotron Laboratory, Michigan State University, East Lansing, MI 48824, USA*
[4] *Sandia National Laboratories, Albuquerque, NM 87185-1189, USA*

ABSTRACT

Magnetized turbulence is ubiquitous in many astrophysical and terrestrial systems but no complete, uncontested theory even in the simplest form, magnetohydrodynamics (MHD), exists. Many theories and phenomenologies focus on the joint (kinetic and magnetic) energy fluxes and spectra. We highlight the importance of treating kinetic and magnetic energies separately to shed light on MHD turbulence dynamics. We conduct an implicit large eddy simulation of subsonic, super-Alfvénic MHD turbulence and analyze the scale-wise energy transfer over time. Our key finding is that the kinetic energy spectrum develops a scaling of approximately $k^{-4/3}$ in the stationary regime as the kinetic energy cascade is suppressed by magnetic tension. This motivates a reevaluation of existing MHD turbulence theories with respect to a more differentiated modeling of the energy fluxes.

Keywords: MHD — methods: numerical — turbulence

1. INTRODUCTION

While our understanding of incompressible hydrodynamic turbulence has significantly advanced over the past decades, many critical questions in the realm of compressible magnetohydrodynamic (MHD) turbulence remain unanswered. This regime is of particular interest in both astrophysics and in terrestrial systems where processes on a huge variety of scales are either governed or at least influenced by MHD turbulence. Astrophysical examples include energy transport in the solar convection zone (Canuto & Christensen-Dalsgaard 1998; Miesch 2005), angular momentum transport and energy release in accretion disks (Balbus & Hawley 1998), the core collapse supernova mechanism (Couch & Ott 2015; Mösta et al. 2015), the interstellar medium with its star-forming molecular clouds (Vázquez-Semadeni 2015; Falgarone et al. 2015; Klessen & Glover 2016), and clusters of galaxies that can be used to determine cosmological parameters (Brunetti & Jones 2015; Brüggen & Vazza 2015). In the terrestrial context, this is of interest for a range of plasma experiments, such as laser-produced colliding plasma flows, Z-pinches, and tokamaks (see, e.g., Tzeferacos et al. 2018; Haines 2011; Mazzucato et al. 2009; Ren et al. 2013).

At the same time, MHD turbulence theory and phenomenology also made significant progress from early isotropic models (Iroshnikov 1964; Kraichnan 1965), to critically balanced turbulence (Sridhar & Goldreich 1994; Goldreich & Sridhar 1995), to dynamic alignment (Boldyrev et al. 2009), but it is still a highly debated topic – see, e.g., Galtier (2016); Beresnyak (2019) for recent reviews. Different theories make a variety of predictions for the scaling of the energy spectra depending on the strength of the mean magnetic magnetic field (either external or local), on the cross helicity (balanced versus unbalanced turbulence), and on the magnetic helicity (encoding the topology of the magnetic field configuration). In the majority of cases scaling predictions are only concerned with the total energy spectrum ($E(k) = E_{\rm kin}(k) + E_{\rm mag}(k)$ with wavenumber k) and assume a moderate or strong background field so that dynamics are differentiated between parallel and perpendicular to the mean field. Thus, there is no differentiation between the kinetic ($E_{\rm kin}(k)$) and magnetic ($E_{\rm mag}(k)$) energy spectra. A complementary theoretical approach to modeling magnetohydrodynamic turbulence is the use of shell models, which are a computationally-inexpensive semi-analytical means of modeling turbulence. Notable examples of this include

Corresponding author: Philipp Grete
grete@pa.msu.edu.

Biskamp (1994); Frick & Sokoloff (1998); Plunian & Stepanov (2007) who also observe, for example, flatter spectra, spectral breaks, and different scaling behavior of the kinetic and magnetic energy spectra. However, the behavior strongly depends on the characteristics of the system being modeled (with, e.g., properties of the system such as a mean magnetic field, helicity and cross helicity contributing significantly to the observed outcomes similarly to the locality of the interactions considered). By contrast to predictions from analytic and semi-analytic modeling efforts, numerous computational studies of magnetized turbulence have reported *different* scaling behavior of kinetic and magnetic energy spectra (Haugen et al. 2004; Moll et al. 2011; Teaca et al. 2011; Eyink et al. 2013; Porter et al. 2015; Grete et al. 2017; Bian & Aluie 2019) and, perhaps even more importantly, different scaling behavior of kinetic and magnetic energy spectra has been reported in observations of the solar wind (Boldyrev et al. 2011).

In order to gain a deeper insight into this discrepancy, we present and analyze the evolution and stationary state of the kinetic and magnetic energy spectra and fluxes separately in the context of an implicit large eddy simulation of ideal MHD turbulence in its simplest configuration (vanishing mean field, cross-helicity, and magnetic helicity). We confirm prior results (Haugen et al. 2004; Moll et al. 2011; Teaca et al. 2011; Eyink et al. 2013; Porter et al. 2015; Grete et al. 2017; Bian & Aluie 2019) that the kinetic and magnetic energy spectra exhibit different scaling behavior. In particular, we find that the kinetic energy spectrum exhibits a scaling close to $k^{-4/3}$ – i.e., it is shallower than the spectra predicted in the theories above, which mostly range between $k^{-3/2}$ and $k^{-5/3}$. We further demonstrate, using a shell-to-shell energy transfer analysis, that this "shallow" kinetic energy spectrum is associated with magnetic tension, which acts to suppress the kinetic energy cascade and provides the major contribution in the energy flux from large to small scales. This result is in marked contrast with incompressible *hydrodynamic* turbulence, where the kinetic energy cascade is the *only* means of transferring energy between scales in a self-similar fashion (which in turn leads to the emergence of the $k^{-5/3}$ scaling) and departures from this expected scaling in hydrodynamic turbulence simulations and experiments have been associated with the existence of "bottlenecks" (Falkovich 1994; Schmidt et al. 2006; Frisch et al. 2008; Donzis & Sreenivasan 2010; Küchler et al. 2019; Agrawal et al. 2020). As such, the results presented in this work demonstrate the rich physics phenomenology that can operate even in the simplest scenarios (vanishing mean field, cross-helicity, and magnetic helicity) where magnetic tension is dynamically important and further serve to highlight the necessary ingredients that MHD turbulence theory and phenomenology should incorporate in order to explain scalings of kinetic and magnetic energy observed in both simulation *and* observation of magnetized turbulence.

The rest of this paper is structured as follows. In Section 2 we introduce the simulation setup and summarize the energy transfer analysis. In Section 3 we present the kinetic and magnetic energy spectra, their temporal evolution, and scale dependent energy dynamics. Finally, in Section 4, we summarize our results, the limitations of the simulations upon which they are based and discuss the implications for both modeling of magnetohydrodynamic turbulence and astrophysical systems.

2. METHOD

2.1. *Simulation setup*

We use the open source code, `K-Athena` (Grete et al. 2021), a performance portable implementation of `Athena++` (Stone et al. 2020) based on `Kokkos` (Edwards et al. 2014), to solve the ideal MHD equations[1]. The second-order finite volume scheme employed is comprised of a Van-Leer integrator, constrained transport MHD algorithm, piecewise-linear reconstruction, and Roe Riemann solver, (see Stone & Gardiner 2009, for more details on the numerical method). Given that no explicit physical dissipative terms are present dissipation is purely numerical; as such the simulations presented here utilize the implicit large eddy simulation (ILES) technique (Grinstein et al. 2007). Turbulent driving is accomplished through a stochastic forcing approach described by (Schmidt et al. 2009), implemented within `K-Athena` using a communication-avoiding algorithm for efficient large scale parallel simulations on GPUs.

We conduct a single simulation of a cubic domain with side length of 1 (if not noted otherwise all units are in code units) and periodic boundary conditions on a $2{,}048^3$ grid. The plasma is initially at rest (velocity $\mathbf{u} = 0$) with uniform density ($\rho = 1$) and thermal pressure ($p_{\rm th} = 1$). The initial magnetic field configuration ($\mathbf{B}_0 = \nabla \times \mathbf{A}_0$ with $\mathbf{A}_0 = (0, 0, r_0 - r)$ for $r < r_0$ with $r = \sqrt{(x-0.5)^2 + (y-0.5)^2}$) is a cylinder in the z-direction with radius $r_0 = 0.4$ and centered in the xy-plane, i.e., there is no magnetic flux going through any of the outer surfaces. The initial magnetic field strength is comparatively weak with $\langle E_{\rm mag} \rangle = 0.00125$ correspond-

[1] `K-Athena` is available at https://gitlab.com/pgrete/kathena. Commit `e5faee49` was used to run the simulation and the parameter file (`athinput.fmturb`) is contained in the supplemental material for this paper.

ing to a plasma beta (ratio of thermal to magnetic pressure) of $\beta_\mathrm{p} = 800$. The plasma is kept approximately isothermal using an adiabatic equation of state with adiabatic index of $\gamma = 1.0001$.

In order to reach a state of stationary turbulence, we employ a large scale mechanical driving force (having an inverse parabolic shape with a peak at $k = 2$, where k is the normalized wavenumber). The driving field is purely solenoidal and has an autocorrelation time of 1.0 so that no artificial compressible modes are injected (Grete et al. 2018). In the stationary regime the integral length is $L = \int E_\mathrm{kin}(k)/k \, \mathrm{d}k / \int E_\mathrm{kin}(k) \mathrm{d}k = 0.32$ (i.e., slightly smaller than the forcing scale at 0.5), the root mean square (RMS) sonic Mach number is $\mathrm{M_s} = 0.54$, the resulting large eddy turnover time is $T = L/(\mathrm{M_s} c_s) = 0.59$, the RMS Alfvènic Mach number is $\mathrm{M_a} = 2.8$, and the mean plasma beta is $\beta_\mathrm{p} = 54$.

2.2. *Energy transfer analysis*

For a detailed analysis of the energy dynamics we apply the shell-to-shell energy transfer analysis presented in Grete et al. (2017), which is an extension of Alexakis et al. (2005) to the compressible regime. The key idea is to separate energy transfers by their source (some energy budget at some spatial scale Q), sink (some budget at some scale K), and a mediator. Given the isothermal nature of the simulation, we focus on the kinetic and magnetic energy budget only and neglect a detailed analysis of the internal energy budget (cf. Schmidt & Grete 2019) or non-isothermal statistics (Grete et al. 2020).

In general, the energy transfers are given by

$$\mathcal{T}_\mathrm{XY}(Q, K) \quad \text{with} \quad \mathrm{X}, \mathrm{Y} \in \{\mathrm{U}, \mathrm{B}\} \tag{1}$$

expressing energy transfer (for $\mathcal{T} > 0$) from shell Q of energy budget X to shell K of energy budget Y. U and B represent the kinetic and magnetic energy budgets, respectively. More specifically, the energy transfers are

$$\mathcal{T}_\mathrm{UU}(Q, K) = -\int \mathbf{w}^\mathrm{K} \cdot (\mathbf{u} \cdot \nabla) \, \mathbf{w}^\mathrm{Q} + \frac{1}{2} \mathbf{w}^\mathrm{K} \cdot \mathbf{w}^\mathrm{Q} \nabla \cdot \mathbf{u} \mathrm{d}\mathbf{x} \tag{2}$$

$$\mathcal{T}_\mathrm{BB}(Q, K) = -\int \mathbf{B}^\mathrm{K} \cdot (\mathbf{u} \cdot \nabla) \, \mathbf{B}^\mathrm{Q} + \frac{1}{2} \mathbf{B}^\mathrm{K} \cdot \mathbf{B}^\mathrm{Q} \nabla \cdot \mathbf{u} \mathrm{d}\mathbf{x} \tag{3}$$

for kinetic-to-kinetic (and magnetic-to-magnetic) transfers via advection and compression,

$$\mathcal{T}_\mathrm{BUT}(Q, K) = \int \mathbf{w}^\mathrm{K} \cdot (\mathbf{v}_\mathrm{A} \cdot \nabla) \, \mathbf{B}^\mathrm{Q} \mathrm{d}\mathbf{x} \tag{4}$$

$$\mathcal{T}_\mathrm{UBT}(Q, K) = \int \mathbf{B}^\mathrm{K} \cdot \nabla \cdot \left(\mathbf{v}_\mathrm{A} \otimes \mathbf{w}^\mathrm{Q}\right) \mathrm{d}\mathbf{x} \tag{5}$$

for magnetic-to-kinetic (and kinetic-to-magnetic) energy transfer via magnetic tension, and

$$\mathcal{T}_\mathrm{BUP}(Q, K) = -\int \frac{\mathbf{w}^\mathrm{K}}{2\sqrt{\rho}} \cdot \nabla \left(\mathbf{B} \cdot \mathbf{B}^\mathrm{Q}\right) \mathrm{d}\mathbf{x} \tag{6}$$

$$\mathcal{T}_\mathrm{UBP}(Q, K) = -\int \mathbf{B}^\mathrm{K} \cdot \mathbf{B} \nabla \cdot \left(\frac{\mathbf{w}^\mathrm{Q}}{2\sqrt{\rho}}\right) \mathrm{d}\mathbf{x} \tag{7}$$

for magnetic-to-kinetic (and kinetic-to-magnetic) energy transfer via magnetic pressure. Here, $\mathbf{w} = \sqrt{\rho}\mathbf{u}$ is a mass-weighted velocity chosen so that the spectral kinetic energy density based on $\frac{1}{2}w^2$ is a positive definite quantity (Kida & Orszag 1990) and $\mathbf{v}_\mathrm{A}$ is the Alfvén velocity.

The velocity $\mathbf{w}^\mathrm{K}$ and magnetic field $\mathbf{B}^\mathrm{K}$ in a shell K (or Q) are obtained by a sharp spectral filter in Fourier space with logarithmic spacing. The bounds are given by 1 and $2^{n/4+2}$ for $n \in \{-1, 0, 1, \ldots, 36\}$. Shells (uppercase, e.g., K) and wavenumbers (lowercase, e.g., k) obey a direct mapping, i.e., $K = 24$ corresponds to $k \in (22.6, 26.9]$.

Given the low sonic Mach number of the simulation (i.e., limited density variations) differences between the shell filtered transfers and transfers obtained through our coarse-graining approach (similar to the formalism employed in large eddy simulations) are expected to be negligible (Aluie 2013; Yang et al. 2016).

3. RESULTS

3.1. *Emergence of a power law in $E_\mathrm{kin}(k)$*

In MHD turbulence simulations (independent of numerical method such as pseudospectral DNS, higher-order finite difference, or finite volume ILES) without a strong mean field ($B_0 \ll \langle u \rangle_\mathrm{RMS}$) and magnetic Prandtl number $\mathrm{Pm} \approx 1$ two important features emerge in the kinetic and magnetic energy spectra when plotted separately, see Figure 1 for a comparison (Haugen et al. 2004; Moll et al. 2011; Teaca et al. 2011; Eyink et al. 2013; Porter et al. 2015; Grete et al. 2017; Bian & Aluie 2019). First, the turbulent dynamo amplifies magnetic fields on all scales, resulting in $E_\mathrm{mag}(k) > E_\mathrm{kin}(k)$ on all scales smaller than the forcing scales. Second, the kinetic energy spectrum develops a power law regime on the magnetically dominated scales with a slope close to -4/3, i.e., shallower than the Kolmogorov slope of -5/3.

In order to understand the emergence of a flatter-than-Kolmogorov slope, indicative of a less efficient energy cascade, we present a single simulation in more detail in the following sections.

3.2. *Time evolution of the energy power spectra*

Figure 2 illustrates the evolution of the mean magnetic and kinetic energies and their ratio over time. First, the

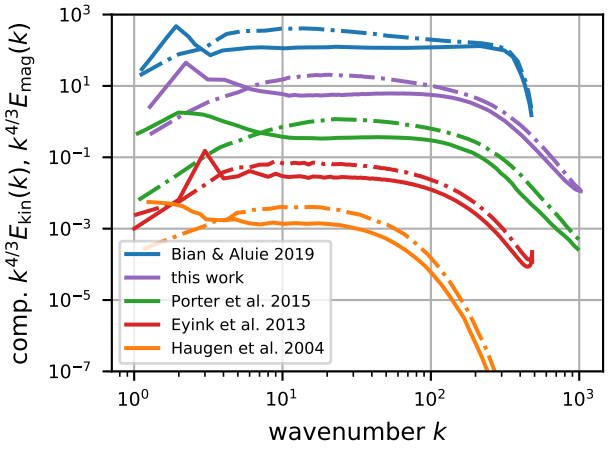


Figure 1. Kinetic (solid) and magnetic (dashed) energy spectra reported in literature from simulations with various numerical schemes, compensated by $k^{4/3}$: pseudo-spectral DNS of incompressible MHD with hyperdissipation(Bian & Aluie 2019, Fig. 10), ILES of compressible, ideal MHD (Porter et al. 2015, Fig. 3) similar to this work, pseudo-spectral DNS of incompressible MHD (Eyink et al. 2013, Fig. 2), and higher-order finite difference DNS of compressible MHD with hyperdissipation (Haugen et al. 2004, Fig. 7). All spectra have in common that magnetic energy dominates all scales smaller than the forcing scale and that the kinetic energy spectrum exhibits a region with scaling close to $k^{4/3}$. (Lines are vertically offset for increased readability.)

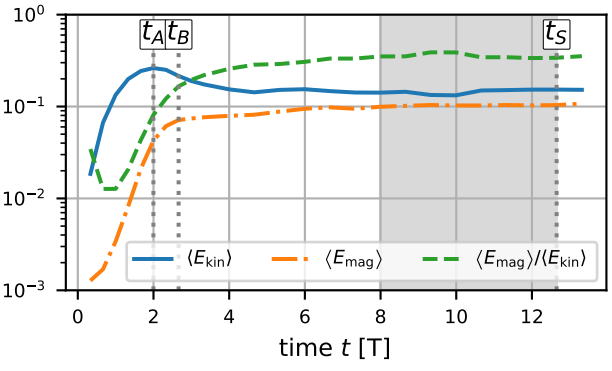


Figure 2. Temporal evolution of mean magnetic energy (orange dash-dotted line), mean kinetic energy (blue solid), and their ratio (green dashed). The shaded gray area indicates the stationary regime. Specific times t_A (peak kinetic energy), t_B (nonlinear dynamo), and t_S (stationary) correspond to snapshots that are analyzed in more detail.

mean kinetic energy reaches its peak value at time t_A.

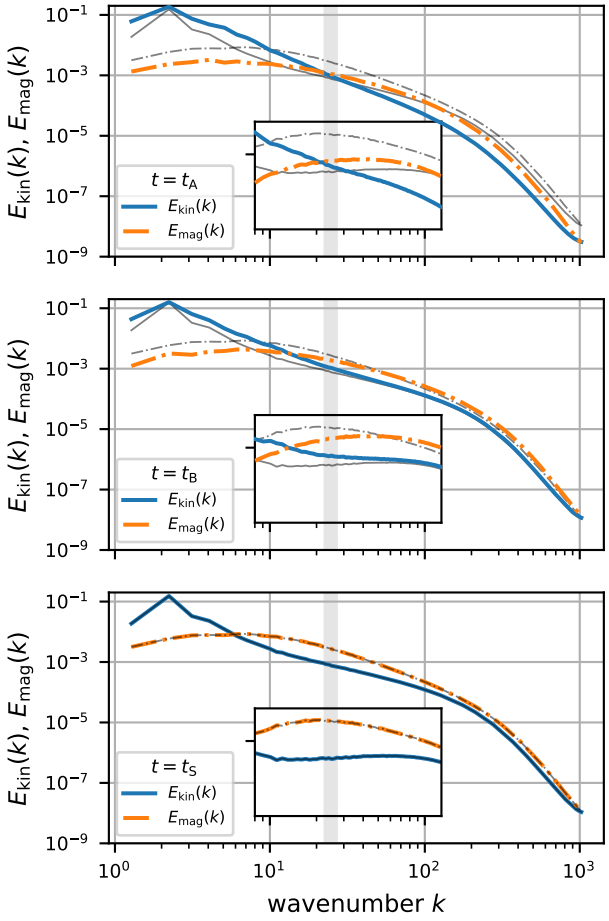


Figure 3. Kinetic (blue solid) and magnetic (orange dash-dotted) energy spectra at different times. The inset shows $8 < k < 64$ compensated by $k^{4/3}$ and illustrates the flattening of the kinetic energy spectrum. The thin lines in each panel illustrate the stationary state (bottom panel) for reference. The gray area at $22.6 < k \leq 26.9$ ($\widehat{=}K = 24$) indicates the scale that is used in the more detailed energy transfer analysis in Section 3.3.

The corresponding spectra[2] (top panel in Figure 3) show that the kinetic energy on small scales ($k \gtrsim 32$) is lower than the stationary value (indicated by the thin black lines), whereas the kinetic energy on large scales is above the stationary value. The magnetic energy spectrum crosses the kinetic energy spectrum at $k_{\rm eq} \approx 24$ (where $E_{\rm kin}(k_{eq}) \approx E_{\rm mag}(k_{eq})$) so that the magnetic field become dynamically relevant on small scales.

At time t_B, which corresponds to the nonlinear phase of the dynamo, the kinetic energy on small scales $k \gtrsim 50$ has reached its stationary value (see center panel in Fig-

[2] A movie of the temporal evolution of the energy spectra (`Grete_et_al-spectra_evol.mp4`) is available in the supplemental material.

ure 3). Moreover, the kinetic energy spectrum shows a first indication of a spectral break around $k \approx 24$ with steeper slope on large scales and a shallower slope on small scales. The crossover of magnetic and kinetic energy has shifted towards larger scales and now occurs around $k_{\mathrm{eq}} \approx 16$.

Finally, the stationary regime is reached after after $\approx 8T$ with E_{mag} saturating at $\approx 0.28 E_{\mathrm{kin}}$. In the stationary regime (represented by $t = t_S$) the crossover has shifted to the largest scales $k_{\mathrm{eq}} \approx 8$ – see bottom panel of Figure 3. Further growth is inhibited due to the large scale purely mechanical force and the magnetic energy is now dominant on all but the largest scales. As a result the kinetic energy spectrum has been significantly flattened and now exhibits a limited range $16 \lesssim k \lesssim 64$ with a shallower-than-Kolmogorov slope close to $\approx -4/3$.

In the following, we demonstrate how magnetic tension is responsible for this flattening of the kinetic energy spectrum by suppressing the kinetic energy cascade.

3.3. *Energy dynamics*

In absence of explicit dissipation (and, thus, the explicit mean dissipation rate), all energy transfer rates are normalized using the mean total cross-scale flux at $k = 26.9$ in the stationary regime as a proxy. This choice has no influence on the actual results, but allows for an easier comparison of relative magnitudes and with other results reported in the literature.

3.3.1. *Magnetic tension*

The role of magnetic tension in shaping the kinetic energy spectrum becomes apparent in Figure 4. It shows the net rate of change in kinetic energy (top row) and magnetic energy (bottom) row for the different mediators over time and for the reference shell $K = 24$, i.e.,

$$\partial_t E^{\mathrm{XY}}_{\mathrm{kin}}(K) = \sum_Q \mathcal{T}_{\mathrm{XY}}(Q, K) \text{ and} \tag{8}$$

$$\partial_t E^{\mathrm{XY}}_{\mathrm{mag}}(K) = \sum_Q \mathcal{T}_{\mathrm{XY}}(Q, K) \tag{9}$$

with XY $\in$ {UU,BUT,BUP} for the kinetic energy and XY $\in$ {BB,UBT,UBP} for the magnetic energy. In other words, this is the net rate of change in energy at some scale K from all other scales Q.

While at time t_A the kinetic cascade ($\mathcal{T}_{\mathrm{UU}}$) is still contributing to a net increase of kinetic energy on those scale, the rate of change by magnetic tension $\mathcal{T}_{\mathrm{BUT}}$ is negative, i.e., removing kinetic energy from $K = 24$. The net effect remains positive. At t_B the dynamics have changed. The kinetic cascade still contributes with a growth in kinetic energy, but magnetic tension now dominates so that the net effect is a removal of kinetic energy from those scales. This transfer of energy from the kinetic to the magnetic budget through magnetic tensions causes the flattening of the kinetic energy spectrum.

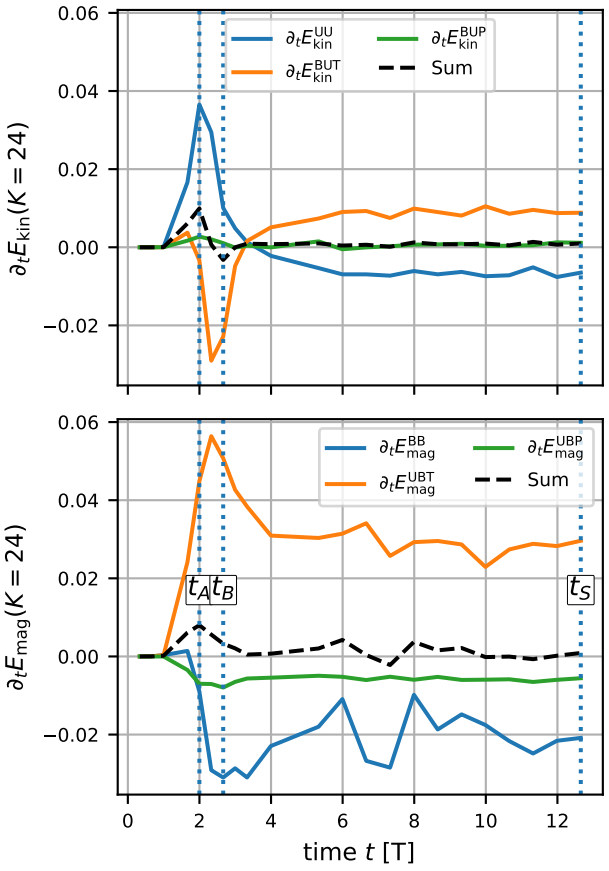


Figure 4. Net rate of change in kinetic (top) and magnetic (bottom) energy at $k = 24$ over time. Blue lines indicate energy transfer through advection, orange through magnetic tension, and green through magnetic pressures. The pressure dilatation and forcing term are not shown as their contribution is negligible.

In the stationary regime the net rate of change in both kinetic and magnetic energy fluctuates around 0 (otherwise the regime should not be considered stationary). This balance is only maintained through energy transfers between kinetic and magnetic energy budgets. On average, the kinetic and magnetic cascades remove energy from intermediate scales of their respective budgets (blue lines are negative) and this deficit is filled through transfers mediated by magnetic tension between budgets (orange lines).

The importance of magnetic tension is similarly observed in the cross-scale energy fluxes. These fluxes are

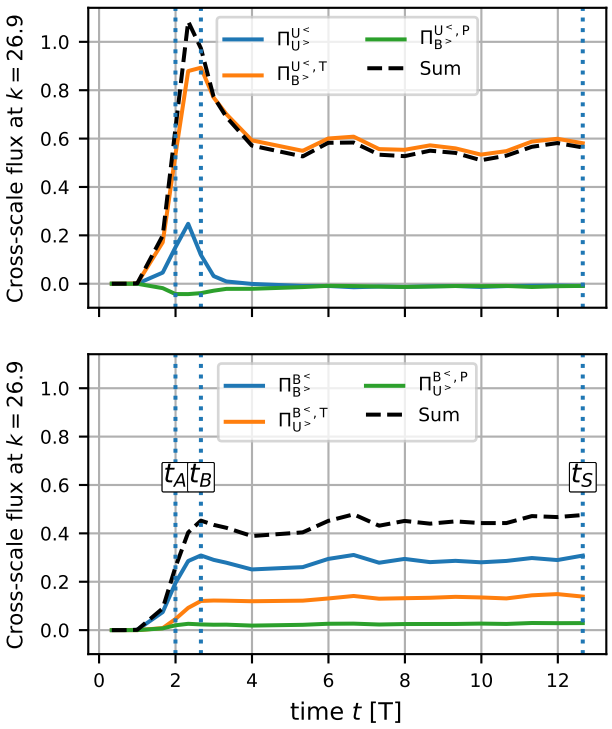


Figure 5. Cross-scale energy transfer across $k = 26.9$ over time, i.e., energy from all budgets going from all larger scales ($k < 26.9$) to the small scale ($k > 26.9$) kinetic budget (top) and magnetic budget (bottom), respectively.

obtained from the individual transport terms via

$$\Pi^{U<}_{U>}(k) = \sum_{Q\le k}\sum_{K>k} \mathcal{T}_{UU}(Q,K)\,, \tag{10}$$

$$\Pi^{U<,T}_{U>}(k) = \sum_{Q\le k}\sum_{K>k} \mathcal{T}_{UBT}(Q,K)\,, \tag{11}$$

$$\Pi^{U<,P}_{U>}(k) = \sum_{Q\le k}\sum_{K>k} \mathcal{T}_{UBP}(Q,K)\,, \tag{12}$$

$$\tag{13}$$

for energy being transferred from the kinetic energy on all scales $\le k$ to to the kinetic and magnetic energies on scales smaller than k by advection, magnetic tension, and magnetic pressure, respectively. The same notation applies to transfers from the large scale magnetic energy with U and B indices exchanged.

Figure 5 illustrates the energy flux across $k = 26.9$ over time from the large scale kinetic energy (top panel) and large scale magnetic energy (bottom panel). Again, the cross-scale flux initially increases in intensity for both of the advection-related transfers (blue lines). While it peaks for $\Pi^{B<}_{B>}$ at t_B and then remains at a constant value, it already peaks for $\Pi^{U<}_{U>}$ at $t = t_A$ and afterwards declines again to 0. Transfers via magnetic tension (orange lines) from both large kinetic and magnetic scales steadily growth till $t = t_B$. Similar to the advection transfers, $\Pi^{B<,T}_{U>}$ remains constant after the peak whereas $\Pi^{U<,T}_{B>}$ declines with the key difference that the decline is not to 0 but to a non-zero value. Moreover, it is the only remaining contribution for the kinetic energy cross-scale flux (at that scale) and, overall, the dominating cross-scale flux is marginally (≈15-20%) stronger than the combined fluxes from the large scale magnetic energy budget by advection and tension. In other words, $\Pi^{U<}_{U>}$, which is the only cross-scale flux in incompressible hydrodynamics, is completely suppressed here and the cross-scale energy transfer transfer from the kinetic energy budget is solely mediated by magnetic tension.

3.3.2. *Large scale energy conversion*

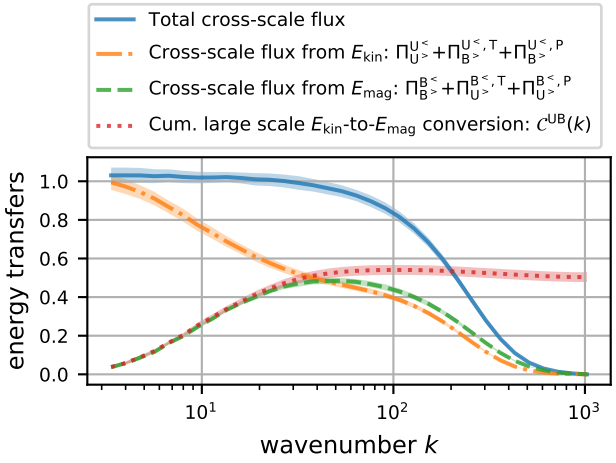


Figure 6. Cross-scale energy transfer across k from the kinetic budget (orange) and magnetic budget (green), and cumulative energy conversion from kinetic to magnetic energy on scales larger than k in the stationary regime.

While cross-scale fluxes allow for intra- (via advection) and inter-budget (via magnetic tension and pressure) transfers, only the latter contributes to a conversion of energy. Figure 6 illustrates the net cross-scale fluxes versus scale in the stationary regime along with the cumulative large scale kinetic to magnetic energy conversion. The cumulative large scale conversion refers to the net energy transfer between those two budgets on all scales larger than the reference scale k,

$$\mathcal{C}^{UB}(k) = \sum_{Q,K\le k} \mathcal{T}_{UBT}(Q,K) + \mathcal{T}_{UBP}(Q,K)\,, \tag{14}$$

where the magnetic pressure contribution is negligible in the simulation presented here. The cumulative energy conversion tightly follows the the cross-scale flux from

the kinetic energy budget. On the largest scales ($k \approx 4$) it is negligible. Here, the cross-scale flux is dominated from the kinetic energy budget as expected in a situation with a large scale mechanical driving. From the large to intermediate scales ($k \approx 30$) the contribution continuously grows while the kinetic energy cross-scale flux contribution decreases. Eventually, the kinetic and magnetic cross-scale fluxes become approximately the same strength. Similarly, the cumulative energy conversion reaches a constant value. This implies that no significant net energy conversion occurs on intermediate and small scales and is in agreement with Bian & Aluie (2019), who show that mean field line stretching is a predominantly large-scale process.

4. SUMMARY, DISCUSSION & CONCLUSIONS

Motivated by an apparent discrepancy between kinetic and magnetic energy spectra scalings measured in simulations (Haugen et al. 2004; Moll et al. 2011; Teaca et al. 2011; Eyink et al. 2013; Porter et al. 2015; Grete et al. 2017; Bian & Aluie 2019) and observations of the solar wind (Boldyrev et al. 2011) with expectations derived from analytic theory (Galtier 2016; Beresnyak 2019), we presented shell-to-shell energy transfer analysis of an implicit large eddy simulation of approximately isothermal, subsonic, super-Alfvénic MHD turbulence with vanishing background magnetic field, cross-helicity, and magnetic helicity. In the context of this analysis, we find that magnetic tension suppresses the kinetic energy cascade resulting in a spectrum that is shallower than predicted in various theories, e.g., $k^{-3/2}$ (Iroshnikov 1964; Kraichnan 1965). Overall, the results presented here demonstrate that the energy flux across scales is dominated by magnetic tension, and similarly the scale local energy balance in the stationary turbulence regime is maintained by a constant energy transfer between the kinetic and magnetic reservoir mediated by magnetic tension.

The simulations on which the results are based, are necessarily limited. While a clear signature of an extended range with a scaling close to $k^{-4/3}$ is observed in the kinetic energy power spectrum, no such range is observed in the magnetic energy power spectrum (see Figure 1). We attribute this to a combination of the simulation setup as well as a limited dynamical range. More specifically, the mechanical energy injection on the largest scales provides a barrier for the large scale magnetic field growth in the absence of a significant (external) mean field. As a result, the magnetic field is strongest on intermediate scales and gets weaker towards larger scales. Similarly, in the limit of large Reynolds numbers we expect the ratio of $E_{\rm mag}(k)/E_{\rm kin}(k)$ to grow from the smallest (non-dissipative) scales towards larger scales until the growth is inhibited by the forcing acting on the largest scales. This also explains why extended scaling ranges are regularly observed in reduced MHD simulations or in simulation with a significant mean field (potentially stronger than the velocity field on the forcing scales) where it, figuratively, provides a large scale anchor, see (Beresnyak 2019).

In this study, we focus on simulations with magnetic Prandtl numbers of $\mathrm{Pm} \simeq 1$ – that is, calculations where the kinetic viscosity and magnetic diffusivity are approximately the same. We note that the results presented here appear to be generally independent of numerical method in the $\mathrm{Pm} \approx 1$ regime. As shown in Figure 1, the scaling in the kinetic energy spectrum has been observed in pseudospectral, finite difference, and finite volume simulations, and with or without explicit (hyper)dissipative terms. While the relative behavior on the smallest scales will depend on Pm, overall it is expected that for $\mathrm{Rm} > \mathrm{Re}$ (i.e., $\mathrm{Pm} > 1$), where magnetic diffusivity is very low compared to kinetic viscosity, magnetic energy will be amplified above the kinetic energy on all scales smaller than the energy injection scale, with the opposite effect happening in the $\mathrm{Pm} < 1$ regime (Brandenburg 2014). While shell models suggest that the the magnetic field will continue to show the behavior we have observed in the $\mathrm{Pm} \gg 1$ regime, at $\mathrm{Pm} \ll 1$ (i.e., when the magnetic diffusion rate is high) it is likely that there will be very little magnetic power at small scales, although the precise details will likely depend on the nature of the turbulent driving. Given that a wide range of magnetic Prandtl numbers are relevant in both terrestrial and astrophysical systems, further work exploring a wider range of Pm is well-motivated.

A further complexity arises when we consider variations in the plasma regime. We are modeling a plasma using the ideal MHD approximation – i.e., assuming that particles are highly collisional, that the Debye length and electron and ion gyroradii are small, and that the inverse of the electron and ion cyclotron frequencies are short compared to the spatial and temporal scales of interest. As these assumptions are relaxed – for example, if the plasma is assumed to be weakly collisional and thus viscosity and resistivity becomes significantly anisotropic – this may impact the results we have observed. Such regimes are important for both terrestrial and astrophysical systems, and while they are beyond the scope of our current efforts they are worthy of consideration. This may require a substantially different numerical approach, however. While some deviations from the ideal MHD regime can be explored with extensions of

the MHD approximation (e.g., adding anisotropic terms as per the Braginskii approximation, Braginskii 1965), it is likely that a kinetic or hybrid fluid/kinetic approximation will be required for some physical regimes.

The key finding of this work is that magnetic tension acts to suppress cross-scale kinetic energy transfer, resulting in a kinetic spectrum with a slope $k^{-4/3}$, in contrast with *theoretical* expectations regarding incompressible hydrodynamic turbulence. Such a suppression of cross-scale kinetic energy transfer is also observed in *simulations* of hydrodynamics turbulence, where the "bottleneck effect" (a pileup of energy on the smallest scales) results in shallower than $k^{-5/3}$ scaling in the kinetic energy spectrum in hydrodynamic turbulence (Falkovich 1994; Schmidt et al. 2006; Frisch et al. 2008; Donzis & Sreenivasan 2010; Küchler et al. 2019; Agrawal et al. 2020). Recently, Gong et al. (2020) also attributed the hydrodynamic bottleneck effect to the shallow kinetic energy spectra they observe in their MHD simulations.

The results presented here demonstrate that, contrary to Gong et al. (2020), the physical mechanism for the shallow slope of the kinetic energy spectrum is *fundamentally* different between hydrodynamics and magnetohydrodynamics due to magnetic tension (which is naturally absent in hydrodynamics) causing a suppression of the kinetic cascade cross-scale flux. In addition, the results presented here suggest that the kinetic cascade is practically absent instead of being decoupled (from a magnetic cascade), as was recently suggested by Bian & Aluie (2019). While we still observe a significant energy flux in the magnetic energy cascade, the balance in the kinetic energy budget is maintained by magnetic tension. Thus, both energy budgets remain coupled through dynamically significant energy fluxes. Note, compared to the vastly extended dynamical range in Bian & Aluie (2019) (which comes from the use of higher-order hyperdisspative terms), the dynamical range in the simulation presented here is rather limited. Future simulations with a larger dynamical range will help to address this question.

With these caveats in mind, the results presented here have a number of implications. First, they motivate a reevaluation of MHD turbulence theories that commonly are only concerned with the total (kinetic and magnetic) energy spectrum and energy flux. In particular, the results presented here suggest that flux-based models should differentiate between the intra- and inter-budget cross-scale fluxes, and consider energy budgets separately. We note that the scaling of the total energy will be dominated by the magnetic energy scaling on intermediate scales, which is important in the light of MHD turbulence theory on scaling relations. Second, in the interpretation of observations and their derived spectra special care is required in inferring properties from one spectra to the other, as we see no indication that that kinetic and magnetic energy spectra follow the same scaling laws, (cf., also Boldyrev et al. 2011). Third, subgrid-scale modeling in the context of large eddy simulations (Miesch et al. 2015; Grete et al. 2016) may become simpler as, for example, one can neglect a purely kinetic cross-scale flux. Finally, we note that in natural systems the effective large scale driving mechanisms, e.g., a galaxy cluster merger (Subramanian et al. 2006), provides an outer scale and limit for the amplification of magnetic fields by the fluctuation dynamo.

Finally, we note that our results should also be interpreted with care and not be overgeneralized. As mentioned in the Introduction, the configuration space of MHD turbulence is vast and the results presented here cover only a single point. Additional data from (even larger-scale) simulations, observations, and experiments is required in order to get a complete picture of MHD turbulence.

ACKNOWLEDGMENTS

The authors thank Jim Stone and Ellen Zweibel for useful discussions. PG and BWO acknowledge funding by NASA Astrophysics Theory Program grant #NNX15AP39G. Sandia National Laboratories is a multimission laboratory managed and operated by National Technology and Engineering Solutions of Sandia LLC, a wholly owned subsidiary of Honeywell International Inc., for the U.S. Department of Energy's National Nuclear Security Administration under contract DE-NA0003525. The views expressed in the article do not necessarily represent the views of the U.S. Department of Energy or the United States Government. SAND Number: SAND2020-9337 O. BWO acknowledges additional funding by NSF grants #1514700, AST-1517908 and AST-1908109, and NASA ATP grant 80NSSC18K1105.

The simulations and analysis were run on the NASA Pleiades supercomputer through allocation SMD-16-7720, on TACC's Stampede2 supercomputer as part of the Extreme Science and Engineering Discovery Environment (XSEDE Towns et al. 2014), which is supported by National Science Foundation grant number ACI-1548562, through allocation #TG-AST090040, and on TACC's Frontera supercomputer through LRAC allocation #AST20004.

The software below is developed by a large number of independent researchers from numerous institutions

around the world. Their commitment to open science has helped make this work possible.

Software: `K-Athena` (Grete et al. 2021), a performance portable version of `Athena++` (Stone et al. 2020) using `Kokkos` (Edwards et al. 2014). `Matplotlib` (Hunter 2007). `NumPy` (van der Walt et al. 2011). `mpi4py` (Dalcn et al. 2005). `mpi4py-fft` (Dalcin et al. 2019).

REFERENCES

Agrawal, R., Alexakis, A., Brachet, M. E., & Tuckerman, L. S. 2020, Phys. Rev. Fluids, 5, 024601, doi: 10.1103/PhysRevFluids.5.024601

Alexakis, A., Mininni, P. D., & Pouquet, A. 2005, Phys. Rev. E, 72, 046301, doi: 10.1103/PhysRevE.72.046301

Aluie, H. 2013, Physica D Nonlinear Phenomena, 247, 54, doi: 10.1016/j.physd.2012.12.009

Balbus, S. A., & Hawley, J. F. 1998, Reviews of Modern Physics, 70, 1, doi: 10.1103/RevModPhys.70.1

Beresnyak, A. 2019, Living Reviews in Computational Astrophysics, 5, 2, doi: 10.1007/s41115-019-0005-8

Bian, X., & Aluie, H. 2019, Phys. Rev. Lett., 122, 135101, doi: 10.1103/PhysRevLett.122.135101

Biskamp, D. 1994, Phys. Rev. E, 50, 2702, doi: 10.1103/PhysRevE.50.2702

Boldyrev, S., Mason, J., & Cattaneo, F. 2009, The Astrophysical Journal, 699, L39, doi: 10.1088/0004-637x/699/1/l39

Boldyrev, S., Perez, J. C., Borovsky, J. E., & Podesta, J. J. 2011, The Astrophysical Journal, 741, L19, doi: 10.1088/2041-8205/741/1/l19

Braginskii, S. I. 1965, Reviews of Plasma Physics, 1, 205

Brandenburg, A. 2014, The Astrophysical Journal, 791, 12, doi: 10.1088/0004-637x/791/1/12

Brüggen, M., & Vazza, F. 2015, Turbulence in the Intracluster Medium, ed. A. Lazarian, M. E. de Gouveia Dal Pino, & C. Melioli (Berlin, Heidelberg: Springer Berlin Heidelberg), 599–614, doi: 10.1007/978-3-662-44625-6_21

Brunetti, G., & Jones, T. W. 2015, Cosmic Rays in Galaxy Clusters and Their Interaction with Magnetic Fields, ed. A. Lazarian, M. E. de Gouveia Dal Pino, & C. Melioli (Berlin, Heidelberg: Springer Berlin Heidelberg), 557–598, doi: 10.1007/978-3-662-44625-6_20

Canuto, V. M., & Christensen-Dalsgaard, J. 1998, Annual Review of Fluid Mechanics, 30, 167, doi: 10.1146/annurev.fluid.30.1.167

Couch, S. M., & Ott, C. D. 2015, ApJ, 799, 5, doi: 10.1088/0004-637X/799/1/5

Dalcin, L., Mortensen, M., & Keyes, D. E. 2019, Journal of Parallel and Distributed Computing, 128, 137 , doi: https://doi.org/10.1016/j.jpdc.2019.02.006

Dalcn, L., Paz, R., & Storti, M. 2005, Journal of Parallel and Distributed Computing, 65, 1108 , doi: https://doi.org/10.1016/j.jpdc.2005.03.010

Donzis, D. A., & Sreenivasan, K. R. 2010, Journal of Fluid Mechanics, 657, 171188, doi: 10.1017/S0022112010001400

Edwards, H. C., Trott, C. R., & Sunderland, D. 2014, Journal of Parallel and Distributed Computing, 74, 3202 , doi: https://doi.org/10.1016/j.jpdc.2014.07.003

Eyink, G., Vishniac, E., Lalescu, C., et al. 2013, Nature, 497, 466, doi: 10.1038/nature12128

Falgarone, E., Momferratos, G., & Lesaffre, P. 2015, The Intermittency of ISM Turbulence: What Do the Observations Tell Us?, ed. A. Lazarian, M. E. de Gouveia Dal Pino, & C. Melioli (Berlin, Heidelberg: Springer Berlin Heidelberg), 227–252, doi: 10.1007/978-3-662-44625-6_9

Falkovich, G. 1994, Physics of Fluids, 6, 1411, doi: 10.1063/1.868255

Frick, P., & Sokoloff, D. 1998, Phys. Rev. E, 57, 4155, doi: 10.1103/PhysRevE.57.4155

Frisch, U., Kurien, S., Pandit, R., et al. 2008, Phys. Rev. Lett., 101, 144501, doi: 10.1103/PhysRevLett.101.144501

Galtier, S. 2016, Introduction to Modern Magnetohydrodynamics (Cambridge University Press), doi: 10.1017/CBO9781316665961

Goldreich, P., & Sridhar, S. 1995, ApJ, 438, 763, doi: 10.1086/175121

Gong, M., Ivlev, A. V., Zhao, B., & Caselli, P. 2020, The Astrophysical Journal, 891, 172, doi: 10.3847/1538-4357/ab744d

Grete, P., Glines, F. W., & O'Shea, B. W. 2021, IEEE Transactions on Parallel and Distributed Systems, 32, 85, doi: 10.1109/TPDS.2020.3010016

Grete, P., O'Shea, B. W., Beckwith, K., Schmidt, W., & Christlieb, A. 2017, Physics of Plasmas, 24, 092311, doi: 10.1063/1.4990613

Grete, P., OShea, B. W., & Beckwith, K. 2018, The Astrophysical Journal Letters, 858, L19. http://stacks.iop.org/2041-8205/858/i=2/a=L19

—. 2020, The Astrophysical Journal, 889, 19, doi: 10.3847/1538-4357/ab5aec

Grete, P., Vlaykov, D. G., Schmidt, W., & Schleicher, D. R. G. 2016, Physics of Plasmas, 23, 062317, doi: 10.1063/1.4954304

Grinstein, F., Margolin, L., & Rider, W. 2007, Implicit Large Eddy Simulation: Computing Turbulent Fluid Dynamics (Cambridge University Press). https://books.google.de/books?id=Xk-eb9kPgXsC

Haines, M. G. 2011, Plasma Physics and Controlled Fusion, 53, 093001. http://stacks.iop.org/0741-3335/53/i=9/a=093001

Haugen, N. E. L., Brandenburg, A., & Dobler, W. 2004, Phys. Rev. E, 70, 016308, doi: 10.1103/PhysRevE.70.016308

Hunter, J. D. 2007, Computing in Science & Engineering, 9, 90, doi: 10.1109/MCSE.2007.55

Iroshnikov, P. S. 1964, Soviet Ast., 7, 566

Kida, S., & Orszag, S. A. 1990, Journal of Scientific Computing, 5, 85, doi: 10.1007/BF01065580

Klessen, R. S., & Glover, S. C. 2016, in Saas-Fee Advanced Course, Vol. 43, Star Formation in Galaxy Evolution: Connecting Numerical Models to Reality, ed. Y. Revaz, P. Jablonka, R. Teyssier, & L. Mayer (Springer Berlin Heidelberg), 85–250, doi: 10.1007/978-3-662-47890-5_2

Kraichnan, R. H. 1965, Physics of Fluids, 8, 1385, doi: 10.1063/1.1761412

Küchler, C., Bewley, G., & Bodenschatz, E. 2019, Journal of Statistical Physics, 175, 617, doi: 10.1007/s10955-019-02251-1

Mazzucato, E., Bell, R. E., Ethier, S., et al. 2009, Nuclear Fusion, 49, 055001, doi: 10.1088/0029-5515/49/5/055001

Miesch, M., Matthaeus, W., Brandenburg, A., et al. 2015, Space Science Reviews, 194, 97, doi: 10.1007/s11214-015-0190-7

Miesch, M. S. 2005, Living Reviews in Solar Physics, 2, doi: 10.1007/lrsp-2005-1

Moll, R., Graham, J. P., Pratt, J., et al. 2011, The Astrophysical Journal, 736, 36. http://stacks.iop.org/0004-637X/736/i=1/a=36

Mösta, P., Ott, C. D., Radice, D., et al. 2015, Nature, 528, 376, doi: 10.1038/nature15755

Plunian, F., & Stepanov, R. 2007, New Journal of Physics, 9, 294, doi: 10.1088/1367-2630/9/8/294

Porter, D. H., Jones, T. W., & Ryu, D. 2015, The Astrophysical Journal, 810, 93, doi: 10.1088/0004-637x/810/2/93

Ren, Y., Guttenfelder, W., Kaye, S. M., et al. 2013, Nuclear Fusion, 53, 083007, doi: 10.1088/0029-5515/53/8/083007

Schmidt, W., Federrath, C., Hupp, M., Kern, S., & Niemeyer, J. C. 2009, Astronomy & Astrophysics, 494, 127, doi: 10.1051/0004-6361:200809967

Schmidt, W., & Grete, P. 2019, Phys. Rev. E, 100, 043116, doi: 10.1103/PhysRevE.100.043116

Schmidt, W., Hillebrandt, W., & Niemeyer, J. C. 2006, Computers & Fluids, 35, 353 , doi: 10.1016/j.compfluid.2005.03.002

Sridhar, S., & Goldreich, P. 1994, ApJ, 432, 612, doi: 10.1086/174600

Stone, J. M., & Gardiner, T. 2009, New Astronomy, 14, 139 , doi: https://doi.org/10.1016/j.newast.2008.06.003

Stone, J. M., Tomida, K., White, C. J., & Felker, K. G. 2020, The Astrophysical Journal Supplement Series, 249, 4, doi: 10.3847/1538-4365/ab929b

Subramanian, K., Shukurov, A., & Haugen, N. E. L. 2006, Monthly Notices of the Royal Astronomical Society, 366, 1437, doi: 10.1111/j.1365-2966.2006.09918.x

Teaca, B., Carati, D., & Domaradzki, J. A. 2011, Physics of Plasmas, 18, 112307, doi: 10.1063/1.3661086

Towns, J., Cockerill, T., Dahan, M., et al. 2014, Computing in Science & Engineering, 16, 62, doi: 10.1109/MCSE.2014.80

Tzeferacos, P., Rigby, A., Bott, A. F. A., et al. 2018, Nature Communications, 9, 591, doi: 10.1038/s41467-018-02953-2

van der Walt, S., Colbert, S. C., & Varoquaux, G. 2011, Computing in Science Engineering, 13, 22, doi: 10.1109/MCSE.2011.37

Vázquez-Semadeni, E. 2015, Interstellar MHD Turbulence and Star Formation, ed. A. Lazarian, M. E. de Gouveia Dal Pino, & C. Melioli (Berlin, Heidelberg: Springer Berlin Heidelberg), 401–444, doi: 10.1007/978-3-662-44625-6_14

Yang, Y., Shi, Y., Wan, M., Matthaeus, W. H., & Chen, S. 2016, Phys. Rev. E, 93, 061102, doi: 10.1103/PhysRevE.93.061102